2015

Absorption properties of type-II InAs/InAsSb superlattices measured by spectroscopic ellipsometry

P T. Webster
Arizona State University at the Tempe Campus

N A. Riordan
Arizona State University at the Tempe Campus

S Liu
Arizona State University at the Tempe Campus

E H. Steenbergen
U.S. Air Force Research Laboratory

R A. Synowicki
J. A. Woollam Co., Inc.

See next page for additional authors

Absorption properties of type-II InAs/InAsSb superlattices measured by spectroscopic ellipsometry

P. T. Webster,[1] N. A. Riordan,[1] S. Liu,[1] E. H. Steenbergen,[2] R. A. Synowicki,[3] Y.-H. Zhang,[1] and S. R. Johnson[1,a)]
[1]*Center for Photonics Innovation and School of Electrical, Computer, and Energy Engineering, Arizona State University, Tempe, Arizona 85287, USA*
[2]*U.S. Air Force Research Laboratory, AFRL/RXAN, Wright Patterson, Ohio 45433, USA*
[3]*J. A. Woollam Co., Inc., 645 M. Street, Suite 102, Lincoln, Nebraska 68508, USA*

(Received 3 December 2014; accepted 4 February 2015; published online 10 February 2015)

Strain-balanced InAs/InAsSb superlattices offer access to the mid- to long-wavelength infrared region with what is essentially a ternary material system at the GaSb lattice constant. The absorption coefficients of InAs/InAsSb superlattices grown by molecular beam epitaxy on (100)-oriented GaSb substrates are measured at room temperature over the 30 to 800 meV photon energy range using spectroscopic ellipsometry, and the miniband structure of each superlattice is calculated using a Kronig-Penney model. The InAs/InAsSb conduction band offset is used as a fitting parameter to align the calculated superlattice ground state transition energy to the measured absorption onset at room temperature and to the photoluminescence peak energy at low temperature. It is observed that the ground state absorption coefficient and transition strength are proportional to the square of the wavefunction overlap and the ground state absorption coefficient approaches a maximum value of around 5780 cm^{-1} as the wavefunction overlap approaches 100%. The absorption analysis of these samples indicates that the optical joint density of states is weakly dependent on the period thickness and Sb content of the superlattice, and that wavefunction overlap is the principal design parameter in terms of obtaining strong absorption in these structures. © *2015 AIP Publishing LLC*. [http://dx.doi.org/10.1063/1.4908255]

Efficient detection in the mid- and long-wavelength infrared is desirable for a variety of applications including gas detection, thermal sensing, astronomy, and infrared spectroscopy. HgCdTe is the dominant infrared detector material used for detecting wavelengths as long as 25 μm,[1] but is fundamentally limited by Auger recombination[2] and must be grown on ternary CdZnTe substrates to obtain high-quality lattice-matched material.[1] Alternatively, superlattice based technologies offer certain advantages over HgCdTe. For example, suppressed Auger recombination has been predicted theoretically and demonstrated experimentally in strained superlattices.[3,4] Furthermore, the heavier electron effective mass which arises as a result of the modified dispersion relation in the superlattice[5] reduces dark current due to band-to-band tunneling.[2,6] The heavier electron effective mass also modifies the density of states, allowing superlattices designed for optimal wavefunction overlap to attain absorption coefficients comparable to bulk material.

Strain-balanced InAs/InAsSb superlattices offer access to the mid- to long-wave infrared region using a ternary material system, while also providing the added benefits of low-defect pseudomorphic growth on a common binary substrate such as GaSb.[7] The type-II band alignment between InAs and InAsSb allows the ground state transition energy of the superlattice to be reduced below the bandgaps of either constituent. Due to the type-II band alignment, the absorption coefficient of the InAs/InAsSb superlattice has a strong dependence on the electron-hole wavefunction overlap, which is governed by the InAsSb composition and period thickness of the strain-balanced superlattice. High quality InAs/InAsSb superlattices have been demonstrated with lifetimes as long as 412 ns[8] and 9 μs[9] at 77 K, and 850 ns[9] at 250 K. It is predicted that a lifetime of 350 ns is all that is required for an infrared photodetector to achieve background-limited operation,[10] making this a very attractive material system for high performance infrared optoelectronic devices.[11]

InAs/InAsSb superlattices designed to achieve a thickness-weighted strain-balance[12] are grown by molecular beam epitaxy on (100)-oriented, 1/4 and full 50 mm GaSb substrates. The samples are grown at temperatures ranging from 400 to 450 °C, and consist of a 500 nm thick GaSb buffer, a 10 nm thick AlSb barrier, a 0.5 to 11 μm thick superlattice region composed of alternating InAs/InAsSb layers, a 10 nm thick AlSb barrier, and a 10 nm thick InAs (sample B only) or GaSb cap; the physical cross section of sample B is shown schematically in Fig. 1. In total, 10 InAs/InAsSb superlattices are studied and are summarized in Table I. Reciprocal space maps verify that with the exception of sample A, the superlattices are pseudomorphic which allows the Sb mole fraction and superlattice period to be acquired simultaneously from the 0th order superlattice peak location and the superlattice satellite peak spacing in the (004)-plane ω-2θ x-ray diffraction scans. Furthermore, because the growth rates of InAs and InAsSb are governed by the In-flux and Poisson's ratio (the negative of the transverse strain over the axial strain), the individual thicknesses of the InAs and InAsSb layers are accurately determined. Strain-balance was not achieved in sample A which was

a)Electronic mail: shane.johnson@asu.edu

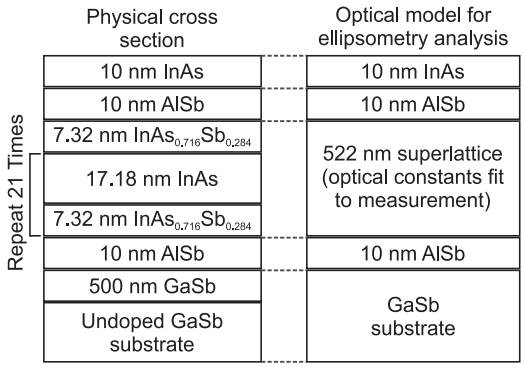

FIG. 1. InAs/InAsSb superlattice sample cross section (sample B, left), alongside the optical model used for ellipsometry analysis (right), which combines the entire superlattice region into a single layer with a unique set of optical constants that are fit to the measured ellipsometric parameters.

found to have relaxed 6.4% towards the InAs lattice constant; this small degree of lattice relaxation is taken into account for the determination of the physical and electronic properties of this sample.

The room temperature optical constants of the superlattice samples are measured using an infrared variable angle spectroscopic ellipsometer[13] that covers the 30 to 800 meV (40 to 1.55 μm wavelength) photon energy range. The GaSb substrate on which the superlattice is grown is transparent over much of this range, making the specular reflections from the backside of the substrate a significant concern. The backside reflections are incoherent with respect to reflections from the epitaxial layers causing a depolarization of the light that reaches the detector. Prior to measurement, the backside of the GaSb wafer is roughened with 320 grit sandpaper to minimize the effect of the backside reflections; the measured depolarization is less than 3% for all samples.

Since the superlattice region has distinctly different optical properties than the materials which compose it, the superlattice is modeled as a single layer with its own unique set of optical constants; the ellipsometric optical model of sample B is shown schematically alongside the physical cross section in Fig. 1. The WVASE software library provides optical constants of the surrounding AlSb layers, the GaSb or InAs cap, and the GaSb buffer and substrate,[14] and the model assumes that there are no reflections from the backside of the substrate. The process of modeling a superlattice as a single layer and fitting its optical constants has been demonstrated in GaAs/AlGaAs[15,16] and InAs/GaInSb[17] superlattices. A wavelength by wavelength analysis[18] of the measured ellipsometric parameters, Ψ and Δ, provides the optical constants, ε_1 and ε_2, and the absorption coefficient ($\alpha = 4\pi k/\lambda$ for extinction coefficient k and photon wavelength λ) of the InAs/InAsSb superlattice. The imaginary part of the wavelength by wavelength complex dielectric function, ε_2, is modeled as a superposition of Gaussian oscillators, from which the real part of the complex dielectric function, ε_1, is generated using the Kramers-Kronig transformation.[19] The generated dielectric function is then compared to the wavelength by wavelength result to verify that the fitted optical constants are Kramers-Kronig consistent. The wavelength by wavelength optical constants and absorption coefficient are used for the analysis that follows.

The superlattice miniband structure and the electron and hole wavefunctions are calculated so that the optical transitions in the superlattice can be attributed to features in the measured room temperature absorption coefficient. The band parameters of InAs and InAsSb are taken from literature,[20–22] the effects of strain are accounted for using the Pikus-Bir Hamiltonian,[23] and the superlattice miniband energies and wavefunctions are calculated using a Kronig-Penney formalism.[24,25] Transition energies are calculated between electron and hole minibands based on crystal momentum conservation, and the electron-hole wavefunction overlap integral indicates which transitions are strongly active in absorption. Since the InAs/InAsSb strained band alignment is not precisely known, the strained conduction band offset is fit for each InAsSb composition to align the calculated ground state transition energy between the first electron and first heavy hole minibands to the measured photoluminescence peak energy at 12 K and to the absorption onset in the measured absorption coefficient spectrum at 295 K.

For each sample in Table I, the ground state absorption onset is taken at the peak in the first derivative of the absorption coefficient spectrum. The value of the absorption

TABLE I. Physical and optical properties of InAs/InAsSb superlattices. The structural properties are measured by x-ray diffraction at 295 K, the absorption properties are measured by spectroscopic ellipsometry at 295 K, and the photoluminescence (PL) peak energy is measured at 12 K. The ground state wavefunction overlap square is calculated using a Kronig-Penney model.

Sample	Sb mole fraction	InAs layer thickness (nm)	InAsSb layer thickness (nm)	Superlattice thickness (μm)	Ground state absorption osnset 295 K (meV)	Ground state absorption coefficient 295 K (cm^{-1})	PL peak energy 12 K (meV)	Ground state wavefunction overlap square 295 K/12 K	Ground state optical joint density of states, 295 K ($\times 10^{18}$ $cm^{-3}eV^{-1}$)
A	0.130	5.13	4.61	0.89	260	3571	318	0.609/0.609	4.26
B	0.284	17.18	7.32	0.52	103	456	161	0.081/0.089	4.47
C	0.312	18.64	5.70	0.96	76	455	131	0.065/0.069	4.34
D	0.328	8.19	2.52	0.98	136	1400	182	0.288/0.281	4.24
E	0.343	15.21	4.67	0.96	74	517	127	0.101/0.105	3.92
F	0.360	18.59	5.72	0.95	56	422	103	0.061/0.061	4.38
G	0.367	15.29	4.71	10.0	51	572	105	0.090/0.094	4.16
H	0.370	14.83	4.56	0.94	64	577	111	0.103/0.103	3.91
I	0.392	7.93	2.46	11.1	107	1645	169	0.277/0.286	4.31
J	0.400	8.31	2.58	0.99	68	1395	145	0.235/0.255	4.44

coefficient at the ground state is taken at the shoulder in the absorption coefficient spectrum, where the first derivative reaches a minimum value prior to the onset of absorption from the next set of minibands. This point in the absorption coefficient spectrum is significant from a band structure perspective, as it corresponds to the point at which the superlattice optical joint density of states (which are the superlattice density of states[26] calculated using the reduced mass of the electron-hole pair in the superlattice[27]) reaches a constant level prior to the onset of the next optical transition.

Fig. 2 shows the absorption coefficient of sample B measured by spectroscopic ellipsometry, with significant wavefunction overlap optical transitions calculated using the Kronig-Penney model shown and labeled in the figure. The onset of absorption occurs at the ground state transition between the first electron and first heavy hole minibands, labeled e_1–hh_1. The square of the wavefunction overlap integral at the ground state of sample B is 8.1%, where the absorption coefficient rises sharply to 456 cm^{-1}. With increasing energy, the absorption coefficient increases in steps with the onsets of higher order optical transitions (e_2–hh_1, e_3–hh_1, e_1–hh_5, etc.), as the density of states increases in steps broadened by the width of the minibands.[26] The selection rule which would forbid some of these transitions in an infinite quantum well is relaxed in the superlattice because the coupled wavefunctions no longer have strictly even or odd parity and because the carriers are primarily localized in different layers as a result of the type-II band alignment. Additionally, the wavefunctions within a miniband are modified with increasing energy through the miniband, resulting in wavefunction overlap integrals with peak values at the energies indicated in the figure and that generally approach zero with increasing or decreasing photon energy; this characteristic of the wavefunction overlap integral is indicated in Fig. 2 via the gray scale gradient shown for each transition.

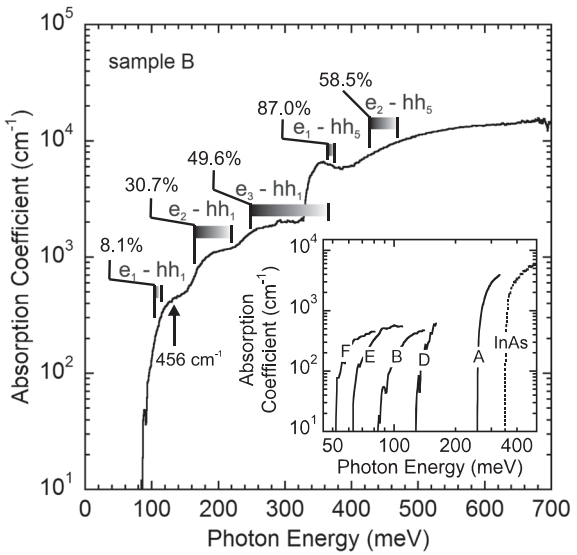

FIG. 2. Room temperature absorption coefficient of an InAs/InAsSb superlattice (sample B) measured by spectroscopic ellipsometry. The optical transitions with significant wavefunction overlap are identified. The maximum of the wavefunction overlap square for each miniband transition is indicated as a percentage, with the gray scale gradient showing how the wavefunction overlap changes with energy. The inset shows the absorption onsets of selected samples along with bulk InAs.

The inset to Fig. 2 shows the ground state absorption onsets of selected samples from Table I which demonstrates that the superlattice can cover a wide range of infrared photon energies from 56 to 260 meV. In addition, the absorption coefficient of bulk InAs is measured and shown as a dotted line for comparison. For a constant period thickness, increasing (decreasing) Sb mole fraction in the InAsSb layers has the effect of increasing (decreasing) the valence band offset of the type-II band alignment of InAsSb and InAs, reducing (increasing) the superlattice ground state cutoff energy. The period thicknesses of samples B, E, and F are comparable, ranging from about 20–25 nm, and the energy shift to decrease in energies is due to the increase in Sb content of each sample (28.4% Sb for sample B, 34.3% Sb for sample E, and 36.0% Sb for sample F). Furthermore, the square of the wavefunction overlap integrals of these three samples are also close in magnitude (8.1% for sample B, 10.1% for sample E, and 6.1% for sample F), owing to the similar period thicknesses of the three samples. The ground state absorption coefficients are also similar in magnitude, with sample E (10.1% wavefunction overlap square) attaining the highest absorption coefficient of the three.

In general, shorter period superlattice designs allow for stronger coupling of the wavefunctions and larger wavefunction overlap. Sample D (32.8% Sb) has an Sb mole fraction between that of samples B (28.4% Sb) and E (34.3% Sb), but has a larger ground state transition energy (136 meV) and larger wavefunction overlap square (28.8%) than samples B or E owing to its significantly shorter period thickness of 10.7 nm. Similar to sample D, sample A also has a relatively short period thickness (9.9 nm compared to 10.7 nm) but with a smaller Sb mole fraction (13.0% Sb compared to 32.8% Sb) resulting in a larger ground state transition energy and wavefunction overlap square (260 meV compared to 136 meV, 60.9% compared to 28.8% wavefunction overlap square).

There is strong shift in the superlattice ground state transition energy with temperature as the constituent material bandgaps significantly decrease with temperature, as can be seen in Table I. Nevertheless, it is observed that the wavefunction overlap in these structures is not significantly affected by temperature. Using the band alignments determined from the room temperature absorption measurements and the low temperature photoluminescence measurements, the calculated wavefunction overlap square at both temperatures is observed to be within 10% for the given superlattice designs. The relative fraction of type-II band alignment distributed to the conduction and valance bands is comparatively constant over these temperatures, resulting in little change in the overlap. This characteristic of the InAs/InAsSb band alignment permits the design of structures with an optimal absorption strength that is not significantly affected by operating temperature. In contrast, the superlattice ground state transition energy is strongly affected by operating temperature.

For each sample presented in Table I, the measured absorption coefficient is used to determine the transition strength,[28] *S*, a dimensionless quantity which provides a

measure of the strength of the optical transition independent of the optical joint density of states

$$S = \left(\frac{2}{m_0}\right)\frac{|\langle\Psi_h|\mathbf{p}|\Psi_e\rangle|^2}{h\nu} = \left(\frac{8\pi^2 m_0}{h^2}\right)(h\nu)|\langle\Psi_h|\mathbf{r}|\Psi_e\rangle|^2. \quad (1)$$

The transition strength can be expressed as a function of either the momentum $\langle\Psi_h|\mathbf{p}|\Psi_e\rangle$ or dipole $\langle\Psi_h|\mathbf{r}|\Psi_e\rangle$ matrix elements.[28,29] The absorption coefficient is also a function of the matrix element. By rearranging the expression for the absorption coefficient,[29] α, the transition strength can be determined from the absorption data by dividing the absorption coefficient by the optical joint density of states, ρ,

$$S = \left(\frac{4m_0 nc\varepsilon_0}{e^2 h}\right)\left(\frac{\alpha}{\rho}\right), \quad (2)$$

where m_0 is the rest mass of the electron, n is the refractive index of the superlattice, c is the speed of light, ε_0 is the vacuum permittivity, e is the electron charge, and h is Planck's constant. The refractive index in the vicinity of the ground state is determined from the spectroscopic ellipsometry measurements to be roughly 3.6 for all samples. For each sample of period thickness d, the transition strength is determined at the highest photon energy within the range of ground state miniband transitions e_1–hh_1, where the optical joint density of states, ρ, reaches its ground state constant level,[25] $\rho_0 = 4\pi m_r/h^2 d$. The reduced mass of the electron-hole pair, $m_r^{-1} = m_e^{-1} + m_{hh}^{-1}$, is determined using the miniband edge electron and heavy hole effective masses, m_e and m_{hh}, respectively. Since the heavy hole effective mass is several orders of magnitude larger than the electron effective mass, the reduced mass of the electron hole pair is just the electron effective mass calculated using the superlattice dispersion relation at the gamma point.[5,30] The dispersion relation in the ground state electron miniband is $E(k) = E_e(1-\cos(kd))/2$, where E_e is the bandwidth of the ground state electron miniband.[5] Taking the second derivative of the dispersion relation with respect to the wave vector k, the electron effective mass and thus the density of states is expressed as a function of the period thickness and the bandwidth of the ground state electron miniband[30]

$$\rho_0 = \frac{2}{\pi E_e d^3}. \quad (3)$$

The calculated values of ρ_0 are listed in Table I for each sample. By substituting ρ_0 and the value of the absorption coefficient α_0 at ρ_0 into Eq. (2), the transition strength for each sample is obtained.

Fig. 3 shows the measured ground state absorption coefficient (left-hand vertical-axis) and the transition strength (right-hand vertical-axis) as a function of the square of the wavefunction overlap integral at the ground state for the samples presented in Table I. The solid lines are linear fits to the absorption coefficient (solid circles) and transition strength (solid squares), with best fit slopes $5780 \pm 370\,\mathrm{cm}^{-1}$ and 45.0 ± 2.9, respectively. The error bars indicate an uncertainty of $\pm 20\%$ in the measured absorption coefficient and the subsequent inferred transition strength. This

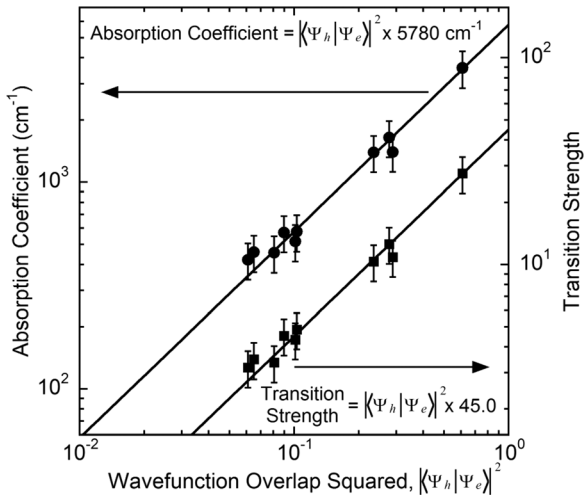

FIG. 3. Room temperature absorption coefficient for the ground state optical transition in strain-balanced InAs/InAsSb superlattices plotted on the left-hand vertical-axis (solid circles) as a function of the square of the wavefunction overlap integral. The transition strength, which is proportional to the absorption coefficient divided by the optical joint density of states, is plotted on the right-hand vertical-axis (solid squares). A unity power law is observed for both sets of data, indicating that the ground state absorption coefficient is proportional to wavefunction overlap squared.

uncertainty is estimated from the sensitivity of the magnitude of the superlattice absorption to the transparency of the GaSb substrate used in the model. For example, the superlattice ground-state absorption coefficient increases by ~10% per $100\,\mathrm{cm}^{-1}$ increase in the absorption coefficient of the substrate. Since the database used in the analysis assumes that the GaSb is transparent over the wavelength range of interest, the presence of any free carrier absorption in the GaSb introduces a small uncertainty in the analysis of the fraction of radiation absorbed in the superlattice. Nevertheless, since it is observed that roughening the substrate backside greatly reduces the intensity of reflected incoherent long wavelength radiation, the GaSb substrates are at least partially transparent ($<100\,\mathrm{cm}^{-1}$), and the presence of free carrier absorption in the substrate is not expected to significantly impact the results.

It is observed that the absorption coefficient and transition strength are proportional to the square of the electron-hole wavefunction overlap, as the variation in the optical joint densities of states of each sample is small (<15% between samples). An increase in the period thickness of the superlattice, which lies in the denominator of the expression for the density of states (Eq. (3)), is partially compensated by the narrowing of the miniband bandwidth which simultaneously decreases due to reduced wavefunction coupling. This compensating effect explains why the densities of states do not change significantly from sample to sample over the range of period thicknesses examined in this study. The validity of Eq. (3) breaks down if the period thickness is very long or very short as the effective mass is no longer accurately described by the bandwidth of the first electron miniband. Extrapolation of the absorption coefficient data in Fig. 3 indicates that as the wavefunction overlap approaches 100%, the ground state absorption coefficient and transition strength of the superlattice approach $5780\,\mathrm{cm}^{-1}$ and 45.0, respectively. The optical joint density of states is weakly

dependent on the superlattice period thickness and Sb mole fraction and is similar in magnitude to that of bulk material.

These results indicate that the optical joint density of states is a minor design parameter in optimizing superlattice absorption. While decreasing the superlattice period thickness of a strain-balanced InAs/InAsSb superlattice does in general lead to improved wavefunction overlap, it also increases the confinement offsets which act to increase the ground state transition energy. As a result, a larger Sb mole fraction is required to keep the ground state transition energy constant while maintaining strain-balance. Increasing Sb mole fraction in the InAsSb layers of the superlattice will increase the confinement of electrons and holes in the superlattice, causing a reduction in wavefunction overlap. Thus, there are two competing effects in the design, increasing wavefunction overlap with decreasing period thickness and decreasing wavefunction overlap with increasing Sb mole fraction, leading to an optimal superlattice design which does not necessarily utilize the smallest period thickness and largest Sb mole fraction to maximize wavefunction overlap. By utilizing wavefunction overlap as a design parameter, the set of superlattice designs which achieve maximum absorption strength can be determined as a function of ground state transition energy. Considering that the wavefunction overlap square values presented in Table I are nearly identical at 12 and 295 K, it is possible that the optimal superlattice design calculated at low temperature will be similar to the optimal design at room temperature. It may then be possible to design a superlattice-based device which maintains optimal absorption over a wide range of operating temperatures.

Ultimately, InAs/InAsSb superlattices are shown to be capable of obtaining absorption coefficients comparable to bulk material despite relying on type-II band alignment to reach longer wavelengths. The period thickness and Sb mole fraction of the superlattice strongly affect the wavefunction overlap and the ground state transition energy and only weakly affect optical joint density of states, indicating that both the ground state cutoff energy and wavefunction overlap are the key design parameters in these structures. The measurement and analysis technique described in this paper provides a means of accurately predicting the expected absorption coefficient as a function of ground state transition energy of the superlattice, and can in principle be performed on any superlattice material system.

In summary, absorption measurements of type-II strain-balanced InAs/InAsSb superlattices show that the ground state absorption coefficient is proportional to the square of the electron-hole wavefunction overlap with an extrapolated value of 5780 cm^{-1} for unity wavefunction overlap.

The authors acknowledge financial support through the U.S. Army Research Office MURI program, Grant No. W911NF-10-1-0524. The authors also acknowledge the use of facilities in the LeRoy Eyring Center for Solid State Science at Arizona State University.

[1]P. Norton, Opto-Electron. Rev. **10**, 159 (2002).
[2]M. A. Kinch, *Fundamentals of Infrared Detector Materials* (SPIE Press, Bellingham, 2007).
[3]C. H. Grein, P. M. Young, and H. Ehrenreich, Appl. Phys. Lett. **61**, 2905 (1992).
[4]E. R. Youngdale, J. R. Meyer, C. A. Hoffman, F. J. Bartoli, C. H. Grein, P. M. Young, H. Ehrenreich, R. H. Miles, and D. H. Chow, Appl. Phys. Lett. **64**, 3160 (1994).
[5]L. Esaki and R. Tsu, IBM J. Res. Dev. **14**, 61 (1970).
[6]D. L. Smith, T. C. McGill, and J. N. Schulman, Appl. Phys. Lett. **43**, 180 (1983).
[7]A. Y. Lew, E. T. Yu, and Y.-H. Zhang, J. Vac. Sci. Technol. B **14**, 2940 (1996).
[8]E. H. Steenbergen, B. C. Connelly, G. D. Metcalfe, H. Shen, M. Wraback, D. Lubyshev, Y. Qiu, J. M. Fastenau, A. W. K. Liu, S. Elhamri, O. O. Cellek, and Y.-H. Zhang, Appl. Phys. Lett. **99**, 251110 (2011).
[9]B. V. Olsen, E. A. Shaner, J. K. Kim, J. F. Klem, S. D. Hawkins, L. M. Murray, J. P. Prineas, M. E. Flatté, and T. F. Boggess, Appl. Phys. Lett. **101**, 092109 (2012).
[10]J. Pellegrino and R. DeWames, Proc. SPIE **7298**, 72981U (2009).
[11]Y.-H. Zhang, Appl. Phys. Lett. **66**, 118 (1995).
[12]N. J. Ekins-Daukes, K. Kawaguchi, and J. Zhang, Cryst. Growth Des. **2**, 287 (2002).
[13]IR-VASE system, J. A. Woollam Co. Inc., Lincoln, NE USA.
[14]E. D. Palik and R. T. Holm, *Handbook of Optical Constants of Solids* (Academic Press, San Diego, 1985).
[15]P. G. Snyder, B. N. De, K. G. Merkel, and J. A. Woollam, Superlatt. Microstruct. **4**, 97 (1988).
[16]J. A. Woollam, P. G. Snyder, K. G. Merkel, and S. A. Alterovitz, Mater. Sci. Eng. B **5**, 291 (1990).
[17]J. Wagner, J. Schmitz, N. Herres, F. Fuchs, and M. Walther, J. Appl. Phys. **83**, 5452 (1998).
[18]M. Schubert, *Infrared Ellipsometry on Semiconductor Layer Structures: Phonons, Plasmons, and Polaritons* (Springer, Heidelberg, 2004), p. 21.
[19]S. L. Chuang, *Physics of Optoelectronic Devices* (Wiley, New York, 1995), pp. 671–674.
[20]I. Vurgaftman, J. R. Meyer, and L. Ram-Mohan, J. Appl. Phys. **89**, 5815 (2001).
[21]G. B. Stringfellow and P. E. Greene, J. Electrochem. Soc. **118**, 805 (1971).
[22]Z. M. Fang, K. Y. Ma, D. H. Jaw, R. M. Cohen, and G. B. Stringfellow, J. Appl. Phys. **67**, 7034 (1990).
[23]S. L. Chuang, *Physics of Optoelectronic Devices* (Wiley, New York, 1995), pp. 655–661.
[24]H.-S. Cho and P. R. Prucnal, Phys Rev. B **36**, 3237 (1987).
[25]S.-H. Pan and S.-M. Feng, Phys. Rev. B **44**, 5668 (1991).
[26]M. W. Prairie and R. M. Kolbas, Superlatt. Microst. **7**, 269 (1990).
[27]S. L. Chuang, *Physics of Optoelectronic Devices* (Wiley, New York, 1995), p. 372.
[28]E. Merzbacher, *Quantum Mechanics* (Wiley, New York, 1970), p. 490.
[29]S. L. Chuang, *Physics of Optoelectronic Devices* (Wiley, New York, 1995), p. 355.
[30]C. Kittel, *Introduction to Solid State Physics* (Wiley, New York, 2005), p. 198.